





Cite this: DOI: 10.1039/d5py00597c

# Biobased multifunctional ingredients for manufacturing tire treads with high mechanical strength and fuel-saving efficiency†

Mingxu Wu,<sup>a,b</sup> Xin He,<sup>a,b</sup> Songbo Zhang,<sup>a,b,c</sup>  <sup>a,b,c</sup> Qizhou Yu,<sup>b,c</sup> Pibo Liu,<sup>b,c</sup> Shuwei Wang  <sup>a</sup> and Yanming Hu<sup>a,b,c</sup>

Energy-saving and environmental sustainability have driven the tire industry to develop high-performance tires, particularly focusing on high energy efficiency and moving towards sustainable materials. Herein, we report the synthesis of a series of biobased sulfur-rich copolymers (SPs) through the inverse vulcanization of plant oils and sulfur, a significant byproduct from the petroleum industry. These SPs serve as multifunctional ingredients for carbon black (CB)-reinforced rubber composites. Leveraging the reactivity of polysulfide segments towards the rubber chain and polycondensed aromatic moieties of CBs as well as the affinity of the functional groups for the oxygenic groups on the CB surface, the biobased SPs act as both reactive plasticizers and interfacial modifiers. Compared to conventional petroleum-based plasticizers, SPs exhibit superior migration resistance and give the resulting composites higher network strength. Meanwhile, incorporation of SPs significantly improves CB dispersion and enhances the interfacial adhesion of SP-based composites, thus leading to high mechanical properties and remarkably decreased hysteresis loss. Especially, the esterified poly(S<sub>30</sub>-ER<sub>70</sub>) shows great potential as a multifunctional ingredient for the preparation of high-performance tires; the poly(S<sub>30</sub>-ER<sub>70</sub>)-based tread composite demonstrates a 16.5% reduction in rolling resistance, 10.7% improvement in wet traction performance, and 13.4% increase in aging resistance, compared to the traditional aromatic oil (AO)-based composite. Moreover, the presence of the dynamic covalent bond (–S–S–) imparts excellent recyclability to the poly(S<sub>30</sub>-ER<sub>70</sub>)-based rubber material.

Received 16th June 2025,

Accepted 12th July 2025

DOI: 10.1039/d5py00597c

rsc.li/polymers

## 1. Introduction

Energy-saving and environmental protection are playing increasingly vital role for the sustainable development of society. Currently, the transportation sector contributes to more than 20% of global energy consumption, with tires, the sole point of contact between the road and a vehicle, accounting for 20 to 30% of a car's fuel consumption. Higher energy consumption directly correlates with increased greenhouse gas emissions.<sup>1,2</sup> Therefore, there is a strong demand for the development of high-performance tires, especially those featuring high energy efficiency. The primary factor affecting a car's energy consumption is rolling resistance, which refers to the energy lost as tires roll along the road.<sup>3</sup> It is well-documented

that, for a given rubber composite, the filler network is the primary determinant of mechanical and dynamic properties, particularly hysteresis, and the hierarchical structure of the filler network primarily depends on the interactions between the fillers and the rubber.<sup>4,5</sup> Among the various fillers used to enhance the mechanical properties of rubber, carbon black (CB) is by far the most applied reinforcing filler in rubber product manufacturing.<sup>6</sup> Unfortunately, CB particles tend to form large agglomerates within hydrophobic rubber matrices owing to strong interparticle van der Waals forces and weak CB-rubber interactions. This results in inferior reinforcing efficiency and high hysteresis loss for the resulting composites as a result of internal friction between CB aggregates.<sup>7</sup> In this context, various modification approaches have been explored to improve CB dispersion and enhance the CB-rubber interaction, including surface modification,<sup>8–10</sup> physical absorption of compatibilizers,<sup>11</sup> and irradiation treatment.<sup>12</sup> However, most of these methods need multiple pretreatment steps or rigorous conditions, making them time-consuming and environmentally unsustainable.

Inverse vulcanization is a facile and effective methodology for converting sulfur, an abundant byproduct of oil refining in the petrochemical industry, into high-value sulfur-rich poly-

<sup>a</sup>School of Textile and Material Engineering, Dalian Polytechnic University, Dalian 116034, China. E-mail: wangshuwei@dipu.edu.cn

<sup>b</sup>Division of Energy Materials, Dalian Institute of Chemical Physics, Chinese Academy of Sciences, Dalian 116023, China. E-mail: zhangsongbo@dicp.ac.cn, ymhu@dicp.ac.cn

<sup>c</sup>Liaoning Key Laboratory of Specialty Polymers, Dalian 116023, China

† Electronic supplementary information (ESI) available. See DOI: <https://doi.org/10.1039/d5py00597c>

mers (SPs).<sup>13–18</sup> These materials exhibit good electrochemical performance and optical properties, enabling their application in Li–S batteries, while their dynamic covalent bonding characteristics contribute to their use in self-healing materials.<sup>19–23</sup> In the field of rubber technology, the Wręczycki and Guo groups reported that SPs could function as effective vulcanizing agents to crosslink diene rubbers.<sup>24,25</sup> Tang *et al.* reported the use of SP derived from sulfur and styrene as an intelligent interfacial modifier in NR/CB composites, which significantly decreased the hysteresis loss and heat build-up by improving CB dispersion and interfacial adhesion.<sup>26</sup> Recently, our group demonstrated that SPs containing alkoxysilyl and hydroxyl moieties could serve as both vulcanizing agents and interfacial modifiers for silica-filled and CB-filled rubber composites to remarkably decrease the rolling resistance and enhance their mechanical properties.<sup>27,28</sup>

Recent advancements have highlighted the potential of renewable biobased resources as alternatives to petroleum-derived monomers in inverse vulcanization.<sup>29–33</sup> It is known that in the production of rubber products, especially automobile tires, which typically contain very large amounts of reinforcing fillers, plasticizers are important ingredients. They help improve filler dispersion, enhance the processability, and improve the flexibility of the final products. Because of non-toxicity, sustainability, and cost-effectiveness, plant oils have gained attention for rubber products, offering a viable replacement to traditional petroleum-based plasticizers, such as aromatic oil (AO), naphthenic oil (NO), and paraffinic oil (PO).<sup>34,35</sup> In particular, thanks to the reactivity of the C=C bonds in plant oils, the mechanical property deterioration, caused by the easy migration and volatilization of traditional petroleum-based plasticizers from rubber products, can be effectively addressed.<sup>36–38</sup> However, the use of reactive biobased plasticizers typically leads to under-sulfurization, where the unsaturated bonds consume the traditional vulcanizing agents (*e.g.*, sulfur) during vulcanization, reducing the crosslink density and tensile modulus of the vulcanizates.<sup>39</sup> This problem can be mitigated through silanization,<sup>40</sup> epoxidation<sup>41</sup> or hydrogenation,<sup>42</sup> although these methods often result in significantly higher costs. We envisioned that this dilemma could be tackled by the synthesis of plant oil-based SPs. Inverse vulcanization of plant oil and sulfur could readily consume the C=C bond(s) completely to address the under-sulfurization problem, while retaining the reactive plasticizer function due to the high reactivity of the produced polysulfide segment with the rubber chains. Moreover, given the strong affinity of the

polar group of the plant oil for CB, the SPs could also serve as an interfacial modifier to improve CB dispersion and its interfacial reaction with rubber matrix, thereby decreasing the rolling resistance of the rubber composite.

In this study, we synthesized a series of biobased SPs through the inverse vulcanization of sulfur with plant oils containing various functional groups (Scheme 1), and these biobased ingredients were adopted as novel reactive plasticizers and interfacial modifiers in CB-filled rubber composites. The function mechanism of the SPs is clarified, and the correlation between their structure and the processing, static and dynamic mechanical properties, and thermo-oxidation aging of the composites were studied in detail. Moreover, the versatility of the SPs in practical application was further evaluated.

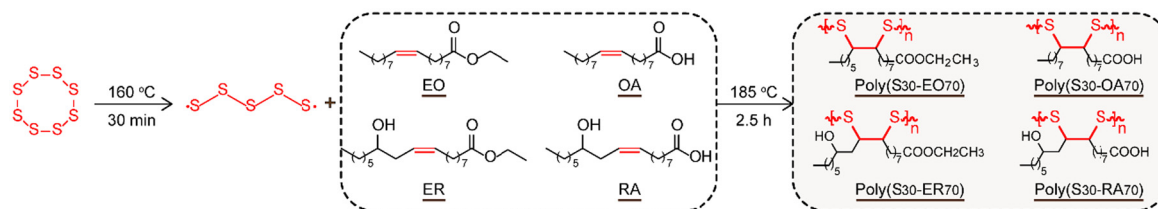
## 2. Experimental section

### 2.1. Materials

Ethyl oleate (EO), oleic acid (OA), and ricinoleic acid (RA) were purchased from Shanghai Macklin Biochemical Co., Ltd, China. Ethyl ricinolate (ER) was obtained from Shanghai Tokyo Chemical Industry Co., Ltd, China. Sulfur (S<sub>8</sub>, 99.5%) was supplied by Damao Chemical Reagent Factory, China. Butadiene isoprene rubber (BIR, Bd : Ip (mol : mol) = 81 : 19, *M*<sub>n</sub> = 131.8 kg mol<sup>−1</sup>, *cis*-1,4-Bd = 97.8%, *cis*-1,4-IP = 98.9%) was synthesized through the coordinative chain transfer copolymerization method as described in our previous study.<sup>43</sup> Solution styrene butadiene rubber (SSBR 2466), carbon black (CB, N330), and rubber additives such as zinc oxide (ZnO, 99%) and stearic acid (SA, 95%), *N*-isopropyl-*N'*-phenyl-1,4-phenylenediamine (4010NA, 98%), aromatic oil (AO, TUDALEN 5192), *N*-cyclohexyl-2-benzothiazole sulfenamide (CBS), 2,2'-dibenzothiazoledisulfide (MBTS), and *N*-tertbutyl-2-benzothiazole sulfenamide (TBBS) were commercially available and used as received.

### 2.2. Synthesis of a series of biobased sulfur-rich copolymers

S<sub>8</sub> (1.5 g) was added to a 20 mL sealed glass vial and heated to 160 °C for 30 min to afford an orange molten polymeric sulfur. Subsequently, 3.5 g of biobased comonomer EO, ER, OA, or RA was added, and the mixture was continuously stirred for 2.5 h at 185 °C, yielding a black-brown copolymer poly(S<sub>30</sub>-EO<sub>70</sub>), poly(S<sub>30</sub>-ER<sub>70</sub>), poly(S<sub>30</sub>-OA<sub>70</sub>), or poly(S<sub>30</sub>-RA<sub>70</sub>), respectively. The copolymer abbreviations reflect the comonomer type and sulfur-to-comonomer mass ratio. The crude product was dis-



**Scheme 1** Synthesis of biobased inverse vulcanized copolymers.

solved in tetrahydrofuran (THF) and purified by filtration and rotary evaporation to yield the target product, and the yields were calculated by gravimetry, which were 95.0%, 91.5%, 93.6%, and 97.4% for poly(S<sub>30</sub>-EO<sub>70</sub>), poly(S<sub>30</sub>-ER<sub>70</sub>), poly(S<sub>30</sub>-OA<sub>70</sub>), and poly(S<sub>30</sub>-RA<sub>70</sub>), respectively.

### 2.3. Preparation of SSBR/CB composites

According to the formulas in Table S1,<sup>†</sup> SSBR, CB, AO, the as-synthesized sulfur-rich copolymers and other rubber additives were sequentially blended on an open two-roll mill (LN-K, Guangdong Lina Industrial Co., Ltd, China). After resting for 12 h, the resultant compounds were compression molded at 150 °C under 12.5 MPa pressure to afford the vulcanized composites, which were named as SSBR/AO, SSBR/poly(S<sub>30</sub>-EO<sub>70</sub>), SSBR/poly(S<sub>30</sub>-ER<sub>70</sub>), SSBR/poly(S<sub>30</sub>-OA<sub>70</sub>), and SSBR/poly(S<sub>30</sub>-RA<sub>70</sub>).

### 2.4. Preparation of tread composites

To illustrate the effectiveness of poly(S<sub>30</sub>-ER<sub>70</sub>) in practical applications, a poly(S<sub>30</sub>-ER<sub>70</sub>)-based tread composite was prepared according to the industrial formulas shown in Table S2.<sup>†</sup> First, SSBR, BIR, activators, antioxidants, CB, and poly(S<sub>30</sub>-ER<sub>70</sub>) were mixed on an open two-roll mill. Then, accelerators and sulfur were further mixed with the compound. After resting for 12 h, the resultant compound was compressed at 150 °C under 12.5 MPa pressure to give the corresponding tread composite, tread/poly(S<sub>30</sub>-ER<sub>70</sub>). For comparison, a BR-based tread composite (BR-tread/AO, BR-tread/poly(S<sub>30</sub>-ER<sub>70</sub>)) was prepared by replacing BIR with BR, and an AO-based tread composite (tread/AO) was prepared by replacing poly(S<sub>30</sub>-ER<sub>70</sub>) with AO.

### 2.5. Characterization

Fourier transform infrared (FT-IR) spectra were recorded in transmission mode on an IR Tracer-100 spectrometer (Shimadzu Co., Ltd, China) scanning the wavenumber range of 400–4000 cm<sup>−1</sup> with 32 scans. The <sup>1</sup>H NMR spectra were collected using a Bruker 400M spectrometer (Bruker Co., Ltd, Germany). Raman spectra were determined by an HNG-ISRaman *In situ* Raman spectroscopy testing system (Shenzhen Haina Optical Technology Co., Ltd, China) with a 355 nm laser. Sulfur content was determined using a Vario EL element analyzer (Elementar, Germany). The molecular weights of the sulfur-rich copolymers were determined using a liquid chromatograph coupled to a high-resolution time-of-flight mass spectrometer (Q-TOF 6540, Agilent Technologies, America). Thermogravimetric analysis (TGA) was performed on a thermogravimetric analyzer (TGA, TA Instrument Co., USA) at a heating rate of 20 °C min<sup>−1</sup> from 30 °C to 700 °C under an N<sub>2</sub> atmosphere.

The intrinsic viscosities of both the aromatic oil and the sulfur-rich plasticizer were determined using a Ubbelohde viscometer using the following equations:

$$[\eta] = \frac{\sqrt{2(\eta_{sp} - \ln \eta_r)}}{c} \quad (1)$$

$$\eta_r = \frac{\eta}{\eta_0} \approx \frac{t}{t_0} \quad (2)$$

$$\eta_{sp} = \eta_r - 1 = \frac{t - t_0}{t_0} \quad (3)$$

where  $[\eta]$  is the intrinsic viscosity,  $\eta_r$  is the relative viscosity,  $\eta_{sp}$  is the specific viscosity,  $c$  is the concentration of the aromatic oil or the sulfur-rich plasticizer solution,  $t$  is the flow time of the aromatic oil or the sulfur-rich plasticizer solution, and  $t_0$  is the flow time of the pure solvent toluene.

Vulcanization characteristics were measured by an MDR-2000E rotorless cure meter (Electronic Wuxi Liyuan Chemical Equipment Co., Ltd, China). The scorch time ( $t_{s1}$ ), cure time ( $t_{90}$ ), minimum torque ( $M_L$ ) and maximum torque ( $M_H$ ) were determined from the curing curve according to ISO 6502. The crosslink densities ( $V_e$ ) of the cured composites were determined by the equilibrium solvent swelling method. The sample was initially weighed ( $m_i$ ) and then immersed in toluene (molar volume  $V_{\text{toluene}} = 106.2 \text{ cm}^3 \text{ mol}^{-1}$ , density  $\rho_{\text{toluene}} = 0.87 \text{ g cm}^{-3}$ ) to swell to equilibrium for 72 h in a swelling tube. The sample was then removed, and the excess toluene was wiped from the surface, and the swelling mass ( $m_{sw}$ ) of the sample was immediately weighed. The solvent was then removed in a vacuum oven at 60 °C to a constant weight ( $m_d$ ). The crosslinking density ( $V_e$ ) was determined by the Flory–Rehner equation:

$$V_e = -\frac{1}{\rho_r v_s} \left[ \frac{\ln(1 - v_r) + v_r + \chi v_r^2}{v_r^{1/3} - \frac{v_r}{2}} \right] \quad (4)$$

For the solvent–elastomer interaction parameter ( $\chi$ ):

$$\chi = 0.34 + \frac{v_s}{RT} (\delta_s - \delta_r)^2 \quad (5)$$

For the volume fraction of the elastomer ( $v_r$ ):

$$v_r = \frac{\frac{m_d}{\rho_r}}{\frac{m_d}{\rho_r} + \frac{m_s}{\rho_s}} \quad (6)$$

where  $\rho_r$  is the density of the vulcanized sample and  $v_s$  is the molar volume of the swelling solvent. Herein,  $v_s$  takes  $106.2 \text{ cm}^3 \text{ mol}^{-1}$ .  $R$  is the universal gas constant ( $1.987 \text{ cal K}^{-1} \text{ mol}^{-1}$ ).  $T$  is the experimental temperature in Kelvin,  $\delta_s$  is the solubility parameter of the solvent ( $\delta_{\text{toluene}} = 8.97 \text{ (cal cm}^{-3})^{-1/2}$ ), and  $\delta_r$  is the solubility parameter of the elastomer ( $8.33 \text{ (cal cm}^{-3})^{-1/2}$ ).  $m_s$  is the equilibrium weight of the swelling solvent ( $m_s = m_{sw} - m_d$ ).  $\rho_r$  and  $\rho_s$  are the densities of rubber and toluene, respectively.  $\rho_r$  is determined according to Archimedes' principle by using a specific gravity balance.

The type and proportion of crosslinking bonds in the poly(S<sub>30</sub>-EO<sub>70</sub>)-based SSBR/BIR vulcanizate were determined in accordance with established literature methodologies.<sup>44</sup> For measurement of the polysulfide crosslinks, a chemical probe solution for dissociation of polysulfide crosslinks was first

made using 0.4 M propane-2-thiol/0.4 M hexylamine in toluene. Then the sample was pre-swollen in toluene for 24 h and then further immersed in the chemical probe solution for 24 h at room temperature under nitrogen atmosphere. After the chemical probe treatment, the sample was immediately soaked in toluene for one day, then moved to fresh toluene and again soaked for one day. After the second swelling, the weight of the swollen sample was measured ( $m_{sw}$ ). The solvent was then dried in a vacuum oven at 60 °C to a constant weight ( $m_d$ ), and the crosslink density ( $V_{e1}$ ) was calculated according to eqn (7)–(9).

The content of polysulfide crosslinks ( $C_{ps}$ ) in total crosslink density was determined by the equation:

$$C_{ps} = \frac{V_{e0} - V_{e1}}{V_{e0}} \times 100\% \quad (7)$$

where  $V_{e0}$  is the total crosslink density of the sample and  $V_{e1}$  is the crosslink density of the sample treated with the chemical probe solution of propane-2-thiol/hexylamine.

The procedure for determining the disulfide crosslinks was similar to that for determining the polysulfide crosslinks. The difference lies in the fact that the chemical probe solution is 2.0 M hexanethiol/4.0 M hexylamine in toluene, which is capable of cleaving both poly- and disulfide crosslinks in vulcanizates.

The content of disulfide crosslinks ( $C_{ds}$ ) was determined by the equation:

$$C_{ds} = \frac{(V_{e0} - V_{e2}) - (V_{e0} - V_{e1})}{V_{e0}} \times 100\% \quad (8)$$

where  $V_{e0}$  is the total crosslink density of the sample,  $V_{e1}$  is the crosslink density of the sample treated with the chemical probe solution of propane-2-thiol/hexylamine, and  $V_{e2}$  is the crosslink density of the sample treated with the chemical probe solution of hexanethiol/hexylamine.

The content of monosulfide and C–C crosslinks ( $C_{C-S/C-C}$ ) was determined by the equation:

$$C_{C-S/C-C} = 100\% - C_{ps} - C_{ds} \quad (9)$$

Differential scanning calorimetry (DSC) analysis of the SPs and rubber composites was performed on a differential scanning calorimeter (DSCQ2000, TA Instrument Co., USA). The samples were sealed in aluminium crucibles and scanned between –60 °C and 40 °C circularly at a rate of 10 °C min<sup>–1</sup> under a N<sub>2</sub> atmosphere. The DSC curves were taken from the second scan. The weight fraction of bound rubber domains  $\chi_{im}$  and the specific heat capacity increment  $\Delta C_{pn}$  for the CB composites were calculated using the equations:

$$\Delta C_{pn} = \frac{\Delta C_p}{1 - w} \quad (10)$$

$$\chi_{im} = \frac{\Delta C_{p0} - \Delta C_{pn}}{\Delta C_{p0}} \times 100\% \quad (11)$$

where  $\Delta C_p$  is the increment of the specific heat capacity at glass transition (W g<sup>–1</sup>),  $\Delta C_{pn}$  is normalized to the weight frac-

tion of the matrix (W g<sup>–1</sup>),  $\Delta C_{p0}$  is the increment of the specific heat capacity for the neat polymer (W g<sup>–1</sup>),  $w$  is the CB weight fraction in the blend, and  $\chi_{im}$  is the bound rubber weight fraction in the composites (wt%).

Torque evolution during the mixing was measured using a HAAKE PolyLab OS Rheo. Drive 7 torque rheometer (HAAKE Co., Ltd, Germany).

The migration stability of the plasticizer was characterized by extraction experiments. Three samples from each group were weighed ( $m_0$ ) and extracted with THF for 48 h in a 250 mL Soxhlet extractor. The sample was dried to constant weight, and the weight was recorded ( $m_e$ ). The extraction rate of the plasticizer is calculated by the equation:

$$E = \frac{\frac{m_0 - m_e}{m_0} - r_a}{r_p} \times 100\% \quad (12)$$

where  $E$  (%) is the extraction rate of the plasticizer,  $r_a$  is the proportion of additives (stearic acid and antioxidant 4010NA) other than plasticizers that can be dissolved by THF in the experimental formula, and  $r_p$  is the proportion of plasticizer in the experimental formula.

The bound rubber content (BRC) of the samples was determined according to the reported method to characterize the interfacial interaction between the rubber matrix and the CB.<sup>45</sup> The bound rubber content was determined by extracting the uncured compounds with toluene for 96 h at ~25 °C, with the solvent renewed every 48 h. The remnants were dried to constant weight under vacuum and subjected to TGA measurement. The bound rubber content (BRC) was calculated as follows:

$$BRC = \frac{W_2 \times P_N}{W_1 \times P_R} \times 100\% \quad (13)$$

where  $W_1$  is the initial mass of the sample and  $W_2$  is the mass of the sample dried to constant weight.  $P_N$  is the mass fraction of nanofiller in the dried sample determined by TGA,  $P_R$  is the mass fraction of rubber in the compound.

The dispersion of nanofiller in the matrix were observed using a Hitachi SU1000 scanning electron microscope (FlexSEM 1000 II, Hitachi High-Technologies Corp., Japan). The accelerating voltage was set to 15.0 kV, and all samples were coated with gold. The particle areas were evaluated by ImageJ software. Strain sweep experiments (storage modulus  $G'$  as a function of the scanning strain) were performed at 60 °C using a rubber process analyzer (RPA-8000, Gotech Testing Machines, Inc., China). The strain amplitude ( $\epsilon\%$ ) varied from 0.1% to 200%, and the frequency was 1 Hz. Dynamic mechanical analysis was performed on a Q800 apparatus (TA Instrument Co., USA), and the samples were heated from –60 °C to 80 °C at 3 °C min<sup>–1</sup> at a frequency of 1 Hz and 0.3% dynamic strain. The mechanical properties of the dumb-bell-shaped composite materials were tested at room temperature at 500 mm min<sup>–1</sup> on a universal testing machine (Changchun Sinter Testing Machine Co., Ltd, China) according to ISO standard 37: 2005.



### 3. Results and discussion

#### 3.1. Synthesis and characterization of biobased SPs

The biobased SPs were synthesized through a typical two-step inverse vulcanization process. Taking poly(S<sub>30</sub>-OA<sub>70</sub>) as a representative example to illustrate the reaction process, elemental sulfur S<sub>8</sub> was initially thermopolymerized into linear polysulfide, as revealed by the color change of molten elemental sulfur from yellow to orange (Fig. S1†). Upon the addition of the comonomer (oleic acid, OA), the initially diphasic mixture gradually transformed into a homogeneous black monophasic as the reaction proceeded, accompanied by a simultaneous increase in viscosity, implying that the reaction between the polysulfide and the C=C bonds on the comonomer proceeded smoothly. The bond connectivity within these SPs was identified using <sup>1</sup>H NMR and FT-IR spectroscopy. In the <sup>1</sup>H NMR spectrum of poly(S<sub>30</sub>-OA<sub>70</sub>) (Fig. 1A), the characteristic signals of the vinyl group (–CH=CH–) at 5.3 ppm and the allyl group (–CH<sub>2</sub>–CH=CH–CH<sub>2</sub>–) at 2.0 ppm disappeared after copolymerization with S<sub>8</sub>. Concurrently, new signals appeared in the range of 2.8–3.8 ppm, corresponding to –S–CH– moieties, indicating the successful copolymerization of elemental sulfur and OA. In addition, the signal centered at 11.0 ppm confirmed the presence of a carboxylic acid group in poly(S<sub>30</sub>-OA<sub>70</sub>).<sup>46</sup> In the FT-IR spectrum (Fig. 1B), the stretching vibration of –CH=CH– at 3008 cm<sup>–1</sup> vanished in poly(S<sub>30</sub>-OA<sub>70</sub>), and new bands for C–H rocking vibrations in the vicinity of C–S (802 cm<sup>–1</sup>)<sup>47</sup> and S–S (438 cm<sup>–1</sup>) emerged. Meanwhile, the band for carbonyl groups (C=O) at 1705 cm<sup>–1</sup> remained. In the Raman spectrum of poly(S<sub>30</sub>-OA<sub>70</sub>) (Fig. S2†), the stretching vibration observed at 350–500 cm<sup>–1</sup> is characteristic of S–S bonds. The successful preparation of poly(S<sub>30</sub>-EO<sub>70</sub>), poly(S<sub>30</sub>-ER<sub>70</sub>), and poly(S<sub>30</sub>-RA<sub>70</sub>) were also confirmed by <sup>1</sup>H NMR and FT-IR spectroscopy (Fig. S3–S5†). It is clear that no sulfur melting peak in the range of 90–120 °C was detected for the as-synthesized sulfur-rich copolymers, implying complete conversion of crystalline sulfur to a polysulfide copolymer (Fig. S6†). The customized structures of these SPs allow them

to function not only as reactive plasticizers but also as potential interfacial modifiers for CB-filled rubber composites (*vide infra*).

Determined by elemental analysis, the mass fractions of S were 28.3%, 30.0%, 29.4%, and 30.3% for poly(S<sub>30</sub>-EO<sub>70</sub>), poly(S<sub>30</sub>-ER<sub>70</sub>), poly(S<sub>30</sub>-OA<sub>70</sub>), and poly(S<sub>30</sub>-RA<sub>70</sub>), respectively, which are close to the designed values. As the biobased comonomers cannot homopolymerize under the described conditions (Fig. S7–S10†), the average S rank of these SPs was calculated to be about 2.0, based on the assumption that each C=C bond forms two C–S bonds. The higher degradation temperatures of the SPs than that of AO (*T*<sub>d5%</sub> = 211–222 °C *vs.* 204 °C) ensure that they are stable during rubber composite processing (Fig. S11†). It is noted that, unlike the polycyclic aromatic hydrocarbons structure of AO (Fig. S12†), the SPs feature long fatty chains and relatively high molecular weights (619–784 g mol<sup>–1</sup>, Fig. S13†). The sulfur-rich polymers exhibit higher intrinsic viscosity values of 2.41 mL g<sup>–1</sup>, 2.82 mL g<sup>–1</sup>, 4.07 mL g<sup>–1</sup>, and 5.47 mL g<sup>–1</sup> for poly(S<sub>30</sub>-EO<sub>70</sub>), poly(S<sub>30</sub>-ER<sub>70</sub>), poly(S<sub>30</sub>-OA<sub>70</sub>), and poly(S<sub>30</sub>-RA<sub>70</sub>), respectively, than that for AO (0.34 mL g<sup>–1</sup>), which is attributable to the increased molecular weight and enhanced intermolecular forces from polar groups (carbonyl group, hydroxyl group, *etc.*). These characteristics enhance their compatibility with the rubber matrix and improve their resistance to migration.<sup>48</sup>

#### 3.2. Plasticization effect, curing reactivity and migration stability of SPs

The plasticization effect of the SPs was investigated by recording the torque evolution during the mixing process. It is known that higher viscosity in rubber compounds generally leads to increased torque response and greater energy consumption during mixing.<sup>49</sup> As shown in Fig. S14,† the incorporation of SPs or AO led to a reduction of the torque in the mixing stage compared with the unplasticized SSBR/CB compound. In particular, the poly(S<sub>30</sub>-EO<sub>70</sub>)-based compound exhibited a 13.5% drop in torque, which is comparable to the effect of the traditional plasticizer AO. This observation

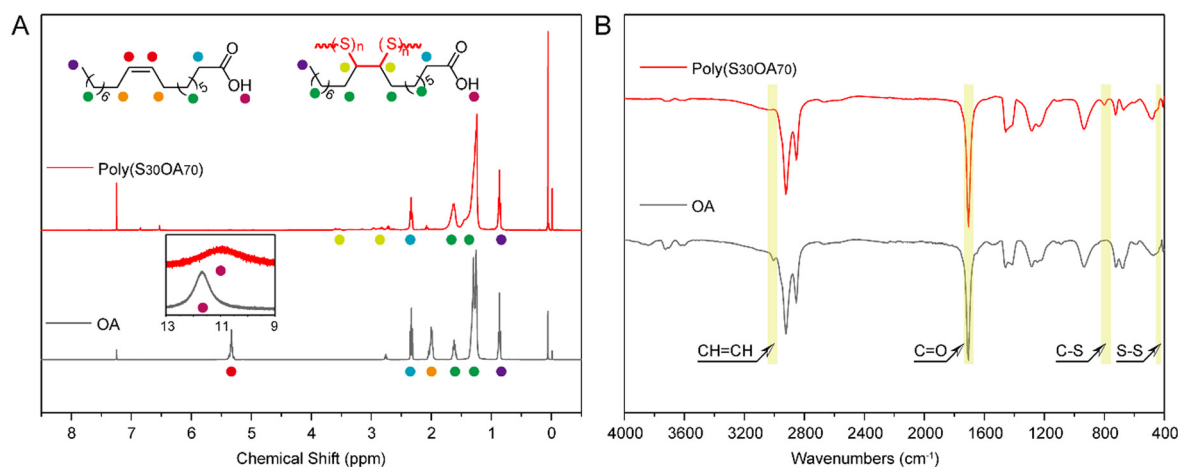


Fig. 1 (A) <sup>1</sup>H NMR and (B) FT-IR spectra of OA and poly(S<sub>30</sub>-OA<sub>70</sub>).

implied that the SPs can indeed act as effective plasticizers like AO, infiltrating the rubber matrix and CB agglomerates to reduce the intermolecular force of the rubber chains and the friction hysteresis between CB particles.

The curing capability of the SPs was examined by monitoring the torque of the rubber compounds on a rheometer (Fig. 2A), and the corresponding curing parameters are summarized in Table S3.† The curing curves of the SSBR composites displayed the typical curing characteristics. The SPs-based plasticizers demonstrate notable vulcanization reactivity with the SSBR chains, resulting in a more pronounced marching modulus behavior in the SPs-based SSBR composites compared to the AO-formulated counterpart. Notably, all the torque differences ( $\Delta M$ , 1.26–1.78 N m) of the SP-based composites were significantly higher than that of the AO-based one, due to the crosslinking agent function of polysulfides as an effective sulfur donor. Therefore, incorporation of the SPs not only enhances the network strength but also mitigates the under-sulfurization issue that is commonly confronted by the unsaturated oil plasticizers, as revealed by the crosslink densities of the SSBR composites (Fig. 2B). All the crosslink densities of SP-based samples are higher than that of the AO-based sample, which is attributed to the polysulfide segments of the SPs being readily thermally activated and subsequently crosslinking with the rubber chains. It is noted that, due to the presence of the acid and hydroxyl groups, the poly( $S_{30}$ -RA<sub>70</sub>)-based SSBR has the highest crosslink density ( $2.61 \times 10^{-4} \text{ mol cm}^{-3}$ ) compared with the SSBR with the acid group consumed (poly( $S_{30}$ -ER<sub>70</sub>)) or no hydroxyl group (poly( $S_{30}$ -OA<sub>70</sub>)). This trend is also observed between poly( $S_{30}$ -ER<sub>70</sub>) and poly( $S_{30}$ -EO<sub>70</sub>). Moreover, highly thermal-oxidation-stable  $-S-C_x-S-$  crosslinks were simultaneously constructed within the SPs-based composites, which may contribute to the enhanced thermal stability (as substantiated below).

For traditional plasticizers, migration is a common issue that can deteriorate the mechanical properties of rubber products. Therefore, the migration effect of the SPs was further

examined by THF extraction, using the AO-based sample for comparison. In contrast to that of the traditional plasticizer AO (99.2%), the migration levels of SPs significantly decrease (31.2%–14.7%) under the same conditions (Fig. 2B). Meanwhile, the migration resistance of the four SPs correlates with their crosslinking abilities in rubber. This is attributed to the reactive nature of the SPs, which integrate into the rubber matrix rather than migrating. These results suggest that the SP-based rubber composites may possess high mechanical stability during storage.<sup>40</sup>

### 3.3. CB dispersion and interfacial interaction in SSBR composites

Given the presence of polysulfide segments and polar moieties (ester, hydroxyl, and carboxyl), these SPs could also function as interfacial modifiers in rubber composites. Fig. 3 shows the cross-sectional morphologies of the vulcanized samples, where the white and gray regions represent the CB particles and rubber matrix, respectively. For SSBR/poly( $S_{30}$ -EO<sub>70</sub>), SSBR/poly( $S_{30}$ -ER<sub>70</sub>), SSBR/poly( $S_{30}$ -OA<sub>70</sub>), and SSBR/poly( $S_{30}$ -RA<sub>70</sub>), the CB dispersion within the rubber matrix appears significantly more uniform compared to that in the SSBR/AO composite, which exhibits localized CB agglomeration. The average size distribution of CB in the SSBR matrix is further obtained using ImageJ software (Fig. S15†), and the results are shown in Fig. 3F. The proportions below 100 nm of CB particles in SSBR/poly( $S_{30}$ -EO<sub>70</sub>), SSBR/poly( $S_{30}$ -ER<sub>70</sub>), SSBR/poly( $S_{30}$ -OA<sub>70</sub>), and SSBR/poly( $S_{30}$ -RA<sub>70</sub>) are 98.7%, 96.0%, 94.9%, and 97.1%, respectively, of the corresponding total CB area, which are higher than that of SSBR/AO (88.4%). This demonstrates the superior efficacy of SPs in enhancing CB dispersion, attributed to their dual functionality as reactive plasticizers and interfacial modifiers.

In addition to the dispersion state, the reinforcing effect of nanofillers is remarkably influenced by the filler–rubber matrix interaction.<sup>50</sup> Such interaction can be determined through detecting heat flow in the glass transition region by

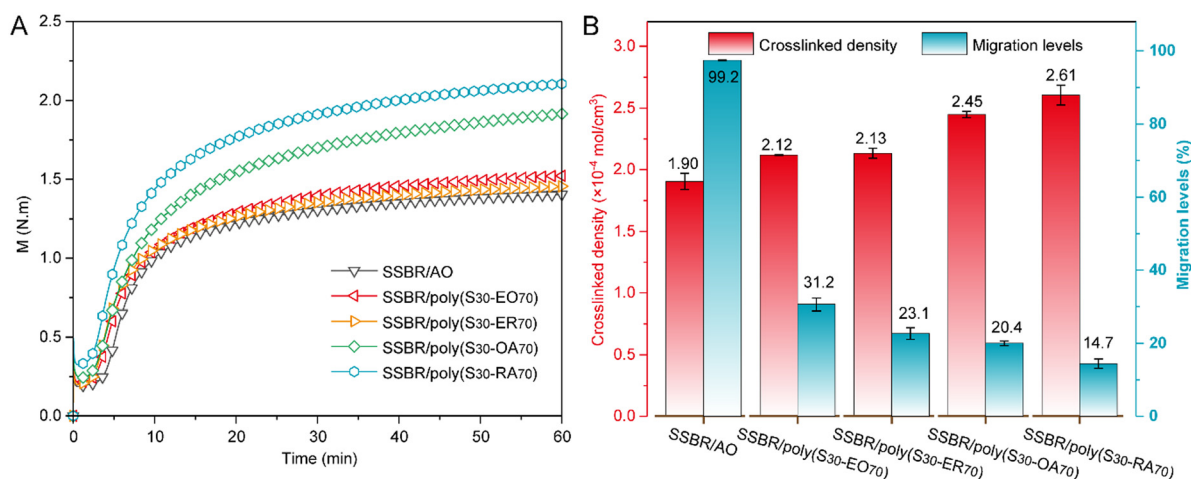


Fig. 2 (A) Curing curves and (B) crosslink densities and migration levels of SSBR composites.

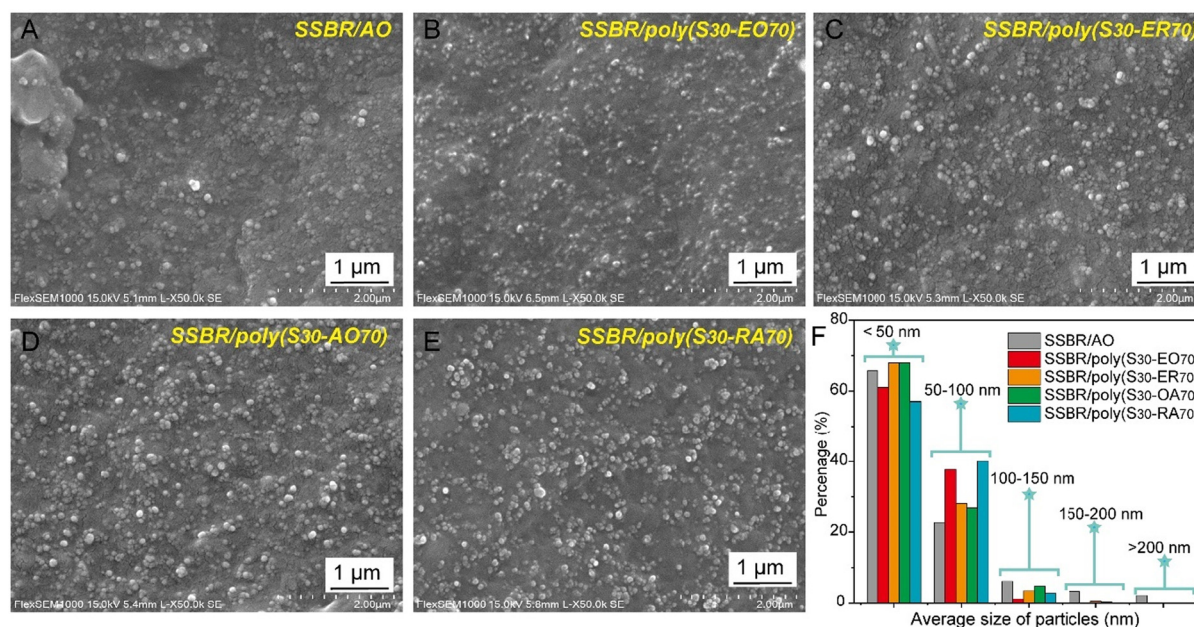


Fig. 3 Cross-sectional morphology of (A–E) CB/SSBR composites and (F) particle statistics.

DSC because the mobility of the rubber chain is sensitive to the local environment.<sup>51</sup> Fig. 4A shows the DSC curves of the SSBR compounds, alongside the calculated values for the specific heat increment ( $\Delta C_{pn}$ ) and weight fraction of constrained rubbers ( $\chi_{im}$ ). For all the SP-based samples, the  $\Delta C_{pn}$  values are lower than that of the SSBR/AO compound. As the  $\Delta C_{pn}$  value is proportional to the number of internal degrees of freedom associated with molecular motion in rubber composites, this reduction suggests an enhanced constrained interface layer fraction formed by the CB–rubber interaction. It is well-known that the filler–rubber interactions result in the occlusion of rubber, leading to “bound rubber”, which restricts chain mobility. As revealed by the  $\chi_{im}$  values, of con-

strained rubber matrix fractions of the SP-based compounds are much higher than that of the SSBR/AO compound, indicating the stronger filler–rubber interactions for the SP-based systems. In particular, because of the higher affinity between the nanofillers and carboxyl groups than that with hydroxyl and ester groups,<sup>50</sup> the SSBR/poly(S<sub>30</sub>-RA<sub>70</sub>) compound exhibits the highest  $\chi_{im}$  value of 24.6 wt%, followed by SSBR/poly(S<sub>30</sub>-OA<sub>70</sub>) (23.0 wt%), SSBR/poly(S<sub>30</sub>-ER<sub>70</sub>) (22.0 wt%), and SSBR/poly(S<sub>30</sub>-EO<sub>70</sub>) (20.9 wt%). Furthermore, as illustrated in Fig. 4B, the bound rubber content, a key metric for evaluating interfacial interactions, follows a comparable pattern, confirming that incorporating SPs significantly reinforces the interfacial bonding between the CB and the SSBR matrix. The

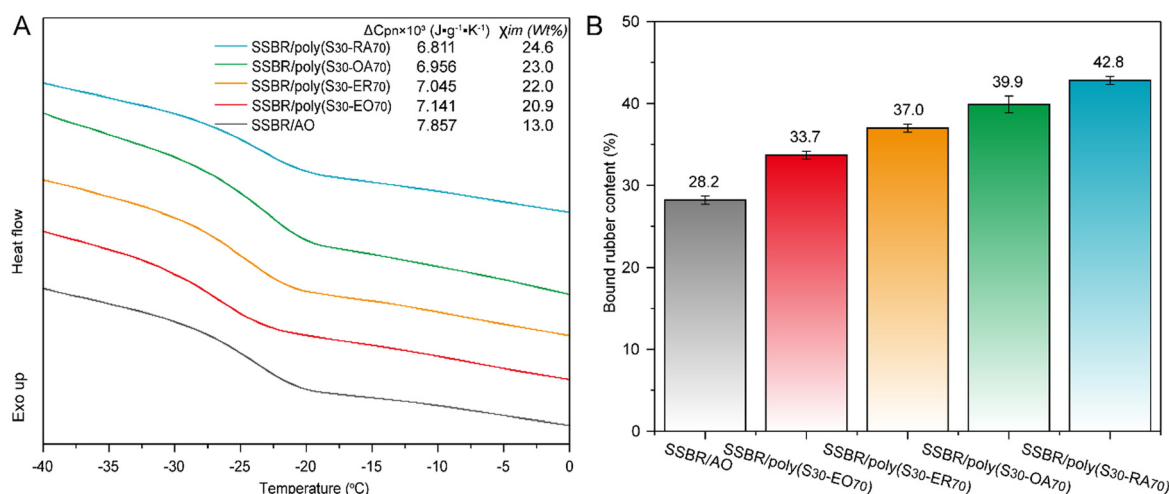


Fig. 4 (A) DSC curves and (B) bound rubber content of the glass transition region of SSBR compounds.



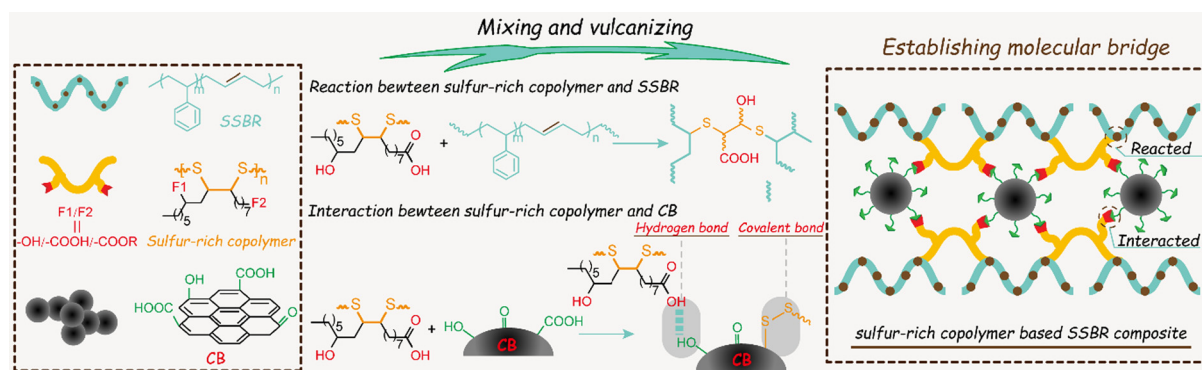
following two points are noteworthy as features of SP-based systems: (i) the polar groups (*i.e.* ester, hydroxyl, carboxyl) can interact with the oxygenic groups on the CB surface through hydrogen bonding,<sup>52</sup> and (ii) the molecular bridge between the rubber chain and the CB can be constructed through the reactions of polysulfide segments with the rubber chain and polycondensed aromatic moieties of the CBs. These synergistic effects strengthen the filler–rubber matrix interaction, promoting tighter adsorption of the rubber chains onto the CB surface (Scheme 2).

### 3.4. Static and dynamic mechanical properties

Fig. 5A shows the stress–strain curves of the SSBR composites, and the mechanical parameters are summarized in Table 1. The modulus at 100% ( $M_{100}$ ) and 300% ( $M_{300}$ ), and tensile strength (TS) of SSBR/poly( $S_{30}$ -EO<sub>70</sub>), SSBR/poly( $S_{30}$ -ER<sub>70</sub>), and SSBR/poly( $S_{30}$ -OA<sub>70</sub>) are all higher than those of the SSBR/AO composite, while the elongation at break (EB) of those SP-based composites are accordingly decreased. This behavior can be attributed to enhanced interfacial interaction and increased crosslink density in the three SP-based composites,

which restrict rubber chain mobility. As a result, the network becomes more constrained, leading to higher modulus and tensile strength but reduced ductility. Interestingly, the TS and EB of SSBR/poly( $S_{30}$ -RA<sub>70</sub>) increase simultaneously by 19.5% (20.2 MPa *vs.* 16.9 MPa) and 6.7% (400% *vs.* 375%), respectively, compared with those of SSBR/AO. This improvement is due to the homogeneous CB dispersion and the enhanced interfacial interaction afforded by the poly( $S_{30}$ -ER<sub>70</sub>), thereby effectively reducing the stress concentration.

Rolling resistance and wet traction are critical performance indicators for tires, reflecting the energy consumption, safety and braking efficiency. The rolling resistance and wet traction correlate well with the corresponding  $\tan \delta$  values at 60 °C and 0 °C, respectively.<sup>45</sup> Generally, a lower  $\tan \delta$  value at 60 °C represents reduced rolling loss (lower energy loss), while a higher value at 0 °C signifies enhanced wet skid resistance. As shown in Fig. 5B, all SP-based composites exhibit lower  $\tan \delta$  values at 60 °C compared to that of the AO-based composite (0.171), indicating reduced hysteresis loss under dynamic working conditions for the SPs-based SSBR composites. Specifically, SSBR/poly( $S_{30}$ -EO<sub>70</sub>) demonstrates the lowest  $\tan \delta$  value at 60 °C



Scheme 2 Schematic for the linkage between SSBR chains and CB built by SPs.

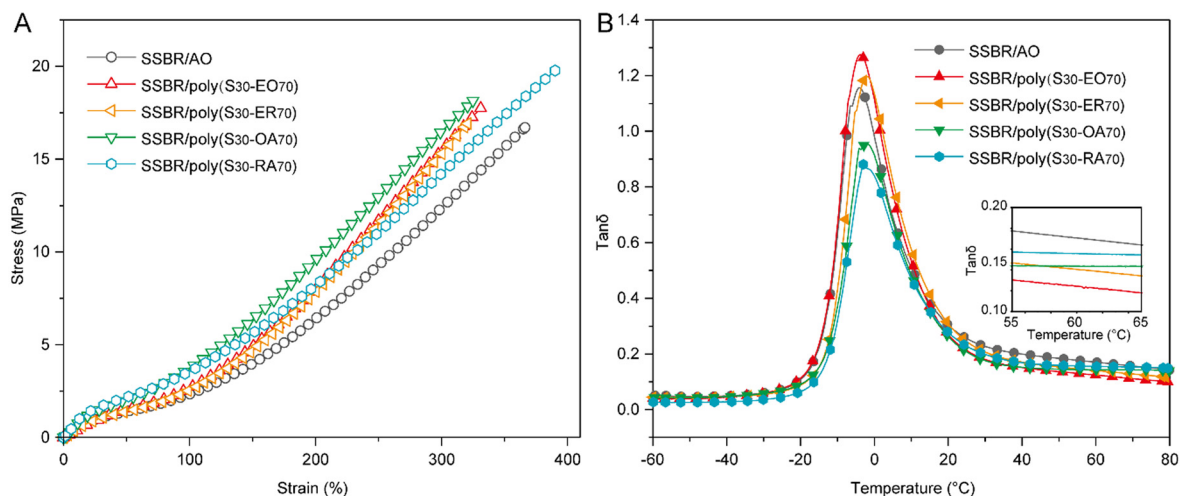


Fig. 5 (A) Stress–strain curves and (B) damping factor ( $\tan \delta$ ) of the SSBR composites as a functions of temperature.



**Table 1** Static and dynamic mechanical parameters of SSBR composites

Sample	$M_{100}^a$ (MPa)	$M_{300}^b$ (MPa)	TS <sup>c</sup> (MPa)	EB <sup>d</sup> (%)	$\tan \delta$ at 0 °C	$\tan \delta$ at 60 °C
SSBR/AO	2.3 ± 0.1	12.2 ± 0.8	16.9 ± 0.9	375 ± 7	0.982	0.171
SSBR/poly(S <sub>30</sub> -EO <sub>70</sub> )	2.8 ± 0.2	16.1 ± 0.6	17.8 ± 0.7	322 ± 10	1.115	0.124
SSBR/poly(S <sub>30</sub> -ER <sub>70</sub> )	2.5 ± 0.1	15.0 ± 0.4	17.5 ± 0.9	341 ± 8	1.135	0.141
SSBR/poly(S <sub>30</sub> -OA <sub>70</sub> )	3.7 ± 0.1	16.3 ± 0.3	17.4 ± 1.0	317 ± 11	0.912	0.144
SSBR/poly(S <sub>30</sub> -RA <sub>70</sub> )	3.5 ± 0.1	14.1 ± 0.2	20.2 ± 0.6	400 ± 14	0.839	0.156

<sup>a</sup>  $M_{100}$  represent the modulus at 100% strain. <sup>b</sup>  $M_{300}$  represent the modulus at 300% strain. <sup>c</sup> TS is the abbreviation for tensile strength. <sup>d</sup> EB is the abbreviation for elongation at break.

(0.124), followed by SSBR/poly(S<sub>30</sub>-ER<sub>70</sub>) (0.141), SSBR/poly(S<sub>30</sub>-OA<sub>70</sub>) (0.144), and SSBR/poly(S<sub>30</sub>-RA<sub>70</sub>) (0.156). This may be attributed not only to the hysteresis effect caused by friction between rubber chains and fillers in the SSBR/POLY(S<sub>30</sub>-ER<sub>70</sub>), SSBR/POLY(S<sub>30</sub>-OA<sub>70</sub>) and SSBR/POLY(S<sub>30</sub>-RA<sub>70</sub>) systems but also to the presence of a hydrogen bond network formed by carboxyl and/or hydroxyl groups, which leads to additional hysteresis losses during dynamic deformation. Conversely, the  $\tan \delta$  values at 0 °C for the two esterified SP-based composites (1.115 for SSBR/poly(S<sub>30</sub>-EO<sub>70</sub>) and 1.135 for SSBR/poly(S<sub>30</sub>-ER<sub>70</sub>)) are higher than that for SSBR/AO (0.982), implying superior wet traction performance. This improvement is attributed to enhanced CB dispersion, which liberates “dead rubber” and increases the fraction of rubber that can engage in the deformation.<sup>53</sup> For the cases of SSBR/poly(S<sub>30</sub>-OA<sub>70</sub>) and SSBR/poly(S<sub>30</sub>-RA<sub>70</sub>), the lower  $\tan \delta$  values at 0 °C compared to that for SSBR/AO might be attributed to the stronger SSBR–CB interfacial interaction, which allows more SSBR chains to be adsorbed onto the CB, reducing the rubber fraction engaging

in dynamic deformation. Given its balanced combination of good rolling resistance and wet traction performance, the esterified SP poly(S<sub>30</sub>-ER<sub>70</sub>) was utilized for further studies.

### 3.5. Application of poly(S<sub>30</sub>-ER<sub>70</sub>) in tread composites

To evaluate the SP in practical applications, we incorporated poly(S<sub>30</sub>-ER<sub>70</sub>) and AO into a BIR-based tread formulation (Table S2†), and the resulting tread was reported to have low rolling resistance and good wear compared with conventional BR-based tread.<sup>43</sup> As expected, tread/poly(S<sub>30</sub>-ER<sub>70</sub>) shows much higher  $\chi_{im}$  than the tread/AO composite (58.0 wt% vs. 42.7 wt%, Fig. S18†). This indicates stronger filler–matrix interaction in the SP-based system. Moreover, the CB dispersity in the tread matrix was evaluated by the “Payne effect”,<sup>54</sup> expressed by the difference ( $\Delta G'$ ) in storage modulus  $G'$  under oscillatory shear strain (Fig. 6A). As the strain amplitude increases, the  $G'$  of the two tread composites decreases due to the breakdown of the CB network. A smaller  $\Delta G'$  value reflects a weaker filler network strength, reflecting better CB dis-

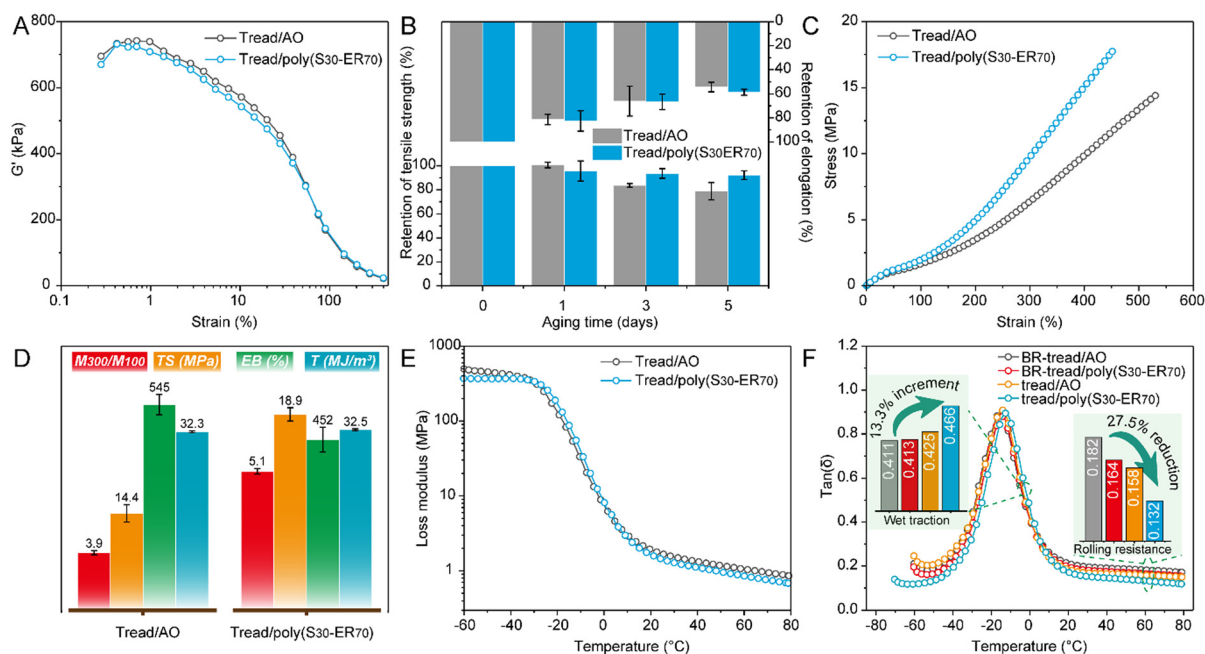


**Fig. 6** (A) Payne effect, (B) thermo-oxidative performance, (C) stress–strain curves, (D) mechanical properties, (E) loss modulus and (F)  $\tan \delta$  as a function of temperature for the tread composites.

persion. Compared with the tread/AO compound, the poly( $S_{30}$ -ER $_{70}$ )-based sample exhibits a weaker "Payne effect", implying the more uniform dispersion of CB. This observation was corroborated by the SEM results (Fig. S19†), which revealed a homogeneous distribution of CB particles in the poly( $S_{30}$ -ER $_{70}$ )-based tread, with no significant agglomerates, in contrast to the tread/AO composite.

Through curing system optimization, the characteristic marching phenomenon during vulcanization was successfully mitigated in the developed tread composites (Fig. S20†). Similar to the SSBR composite mentioned above, owing to uniformly dispersed CB and stronger interfacial interaction with the rubber matrix as well as the curing ability of poly( $S_{30}$ -ER $_{70}$ ), the tread/poly( $S_{30}$ -ER $_{70}$ ) composite has a stronger network than that of the sample based on the traditional plasticizer AO. These factors collectively create a more constrained and rigid network structure, endowing the tread/poly( $S_{30}$ -ER $_{70}$ ) composite with higher tensile strength (TS) and decreased elongation at break (EB) (Fig. 6C and D). Moreover, as shown in Fig. S21,† the tread/poly( $S_{30}$ -ER $_{70}$ ) exhibited a higher tensile strength (18.9 MPa vs. 13.0 MPa) but a lower elongation at break (452% vs. 531%) than that of tread/ER, implying the necessity of inverse vulcanization techniques. The reinforcing

efficiency was evaluated using the reinforcing index (RI), defined as the ratio of  $M_{300}$  to  $M_{100}$  (Fig. 6D). The RI for the tread/poly( $S_{30}$ -ER $_{70}$ ) was 5.1, which was 30.7% higher compared to that of the tread/AO composite (RI = 3.9). This significant improvement implies the enhanced reinforcing effect provided by poly( $S_{30}$ -ER $_{70}$ ).

Considering the excellent migration resistance and the high bond energy of the  $-S-C_x-S-$  crosslinks constructed by poly( $S_{30}$ -ER $_{70}$ ), we anticipate that the aging resistance of the tread composite could be significantly improved. To prove this notion, the anti-aging performance of the tread/poly( $S_{30}$ -ER $_{70}$ ) composite was examined, along with tread/AO for comparison (Fig. 6B, S22 and S23†). After accelerated aging at 100 °C for 5 d, the tread/poly( $S_{30}$ -ER $_{70}$ ) composite retained 92.2% of its tensile strength and 58.6% of its elongation at break, higher than those of the tread/AO composite (78.8% and 54.3%). Moreover, the tread/poly( $S_{30}$ -ER $_{70}$ ) displays a lower loss modulus in the temperature range of 20–80 °C compared with that for the tread/AO composite (Fig. 6E), indicating the reduction of dynamic hysteresis. As shown in Fig. 6F, the tread/AO composite has a lower  $\tan \delta$  value at 60 °C (0.158 vs. 0.182) and a higher  $\tan \delta$  value at 0 °C (0.425 vs. 0.411) with respect to the BR-tread/AO composite, demonstrating the low

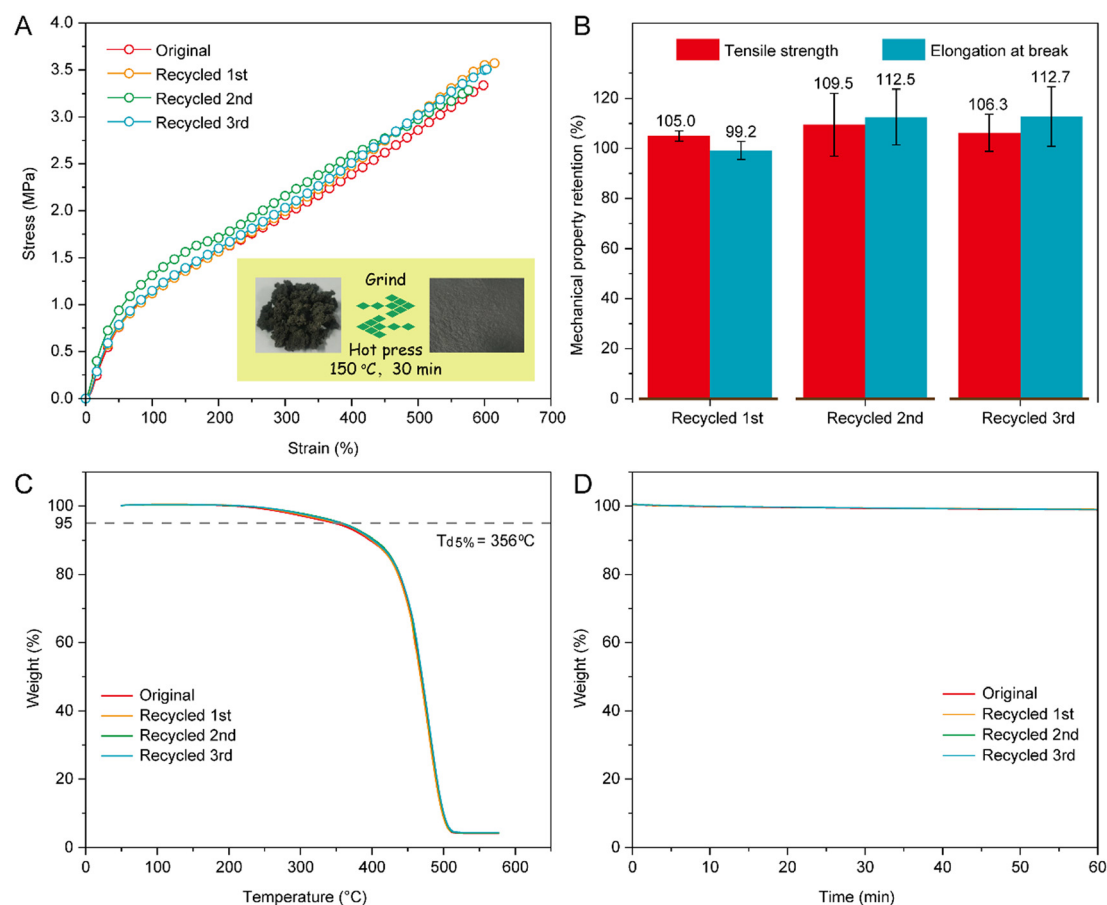


**Fig. 7** (A) Stress–strain curves, (B) retention of tensile strength and elongation, (C) TGA curves as function of the temperature, (D) isothermal curves at 150 °C of the original and recycled poly( $S_{30}$ -EO $_{70}$ )-based SSBR/BIR samples.

rolling resistance and good wet traction of the BIR-based tread compared to those of the BR-based tread. Especially, the rolling resistance of the tread/poly( $S_{30}$ -ER $_{70}$ ) composite, as measured by  $\tan \delta$  at 60 °C, is 16.5%, 19.5% and 27.5% lower than that of tread/AO, BR-based tread/poly( $S_{30}$ -ER $_{70}$ ) and BR-based tread/AO, respectively (0.132 vs. 0.158, 0.164 and 0.182, Fig. 6F). This reduction in rolling resistance is expected to translate into a 4–6% decrease in tire fuel consumption. Tread/poly( $S_{30}$ -EO $_{70}$ ) also exhibits higher wet traction performance, as revealed by a 10.7%, 12.8% and 13.3% increase of  $\tan \delta$  at 0 °C than that of tread/AO, BR-based tread/poly( $S_{30}$ -ER $_{70}$ ) and BR-based tread/AO. Thus, the biobased SPs, especially poly( $S_{30}$ -ER $_{70}$ ), effectively enhance energy efficiency during mixing, improve nanofiller dispersion, and provide exceptional anti-aging properties in rubber composites. These attributes make them highly promising as multifunctional ingredients for the production of high-performance tires.

The presence of dynamic covalent bonds (–S–S–) in the polysulfide-cross-linked rubber system, as demonstrated in our previous study,<sup>27,55</sup> enables exceptional reprocessability. To evaluate the reprocessability, tensile tests were conducted on a poly( $S_{30}$ -EO $_{70}$ )-based SSBR/BIR vulcanizate (formulation in Table S5†). It was confirmed that approximately 80.6% polysulfide crosslinks and 4.6% disulfide crosslinks exist in the poly( $S_{30}$ -EO $_{70}$ )-based SSBR/BIR vulcanizate (Fig. S24†). Reprocessing involved grinding the sample into granules followed by remolding at 150 °C for 30 min under 12.5 MPa pressure. As shown in Fig. 7A, the reprocessed SSBR/BIR vulcanizates retained a defect-free appearance, and their stress-strain curves after 1–3 reprocessing cycles nearly overlapped with the original sample. Remarkably, the mechanical property retention exceeded 105.0% for tensile strength and 99.2% for elongation at break compared to the original sample (Fig. 7B), highlighting outstanding reprocessability and recyclability. Thermal stability during reprocessing was confirmed by the TGA curves of the SSBR/BIR samples, which exhibited a 5% mass loss temperature of ~356 °C (Fig. 7C). Furthermore, the results of isothermal TGA at 150 °C for 1 h under air revealed negligible weight loss (Fig. 7D), confirming robust thermal stability during reprocessing. Thus, adopting inverse vulcanized poly( $S_{30}$ -EO $_{70}$ ) to replace conventional sulfur provided a new avenue to settle the environmental pollution problem caused by waste vulcanized rubber. This work provides a promising solution to address the environmental pollution challenges posed by waste vulcanized rubber, offering a sustainable pathway for rubber recycling and reuse.

## 4. Conclusions

In summary, a series of biobased sulfur-rich copolymers (SPs) were readily synthesized through the inverse vulcanization of sulfur and various plant oils. The unique structural features enable them to function as both reactive plasticizers and interfacial modifiers in rubber composites. The polysulfide segments of SPs can be thermally activated and generate sulfur

radical to react with the rubber matrix, and their polar groups (ester, hydroxyl, and carboxyl) can interact with the oxygenic groups on the CB surface through hydrogen bonding, enabling the construction of a molecular bridge between the rubber chain and the CB particles. As a consequence, SPs display comparable plasticization efficiency to the traditional petroleum plasticizer AO in rubber compounds, while significantly improving migration resistance. It also demonstrated that the CB dispersion within the composites is greatly improved and interfacial interaction is strengthened, as evidenced by the SEM and DSC measurements. These enhancements lead to superior mechanical properties and reduced rolling resistance in SP-based composites compared to AO-based ones. Moreover, the SPs provide great potential for practical applications. The incorporation of poly( $S_{30}$ -ER $_{70}$ ) into a tread composite significantly enhanced the mechanical properties, aging resistance, wet traction, and rolling resistance. Furthermore, the dynamic covalent bond (–S–S–) in the poly( $S_{30}$ -ER $_{70}$ )-based rubber material facilitates its reprocessing and recycling. Overall, this work provides a methodology for the sustainable development of multifunctional ingredients for high-performance tires featuring safety and fuel-saving efficiency.

## Conflicts of interest

There are no conflicts to declare.

## Data availability

The data supporting this article have been included as part of the ESI.†

## Acknowledgements

This work was financially supported by the National Natural Science Foundation of China (Grant No. 52403147) and the National Key R&D Program of China (Grant No. 2022YFB3704704).

## References

- 1 S. Deng, R. Chen, S. Duan, Q. Jia, X. Hao and L. Zhang, *SusMat*, 2023, **3**, 581–608.
- 2 T. Hennequin, L. van Vlimmeren, S. Mostoni, F. R. Pomilla, R. Scotti, C. Stauch, M. K. van der Hulst, M. A. J. Huijbregts and R. van Zelm, *ACS Sustainable Chem. Eng.*, 2024, **12**, 6102–6110.
- 3 E. S. Rødland, G. Binda, D. Spanu, S. Carnati, L. R. Bjerke and L. Nizzetto, *J. Hazard. Mater.*, 2024, **476**, 135042.
- 4 D. Dhara, M. A. Rahman, E. Ruzicka, A. Karekar, D. Vlassopoulos, K. Saalwächter, B. Benicewicz and S. K. Kumar, *Macromolecules*, 2024, **57**, 1448–1460.

- 5 L. A. Wilke, C. G. Robertson, D. A. Karsten and N. J. Hardman, *Carbon*, 2023, **201**, 520–528.
- 6 B. P. Chang, A. Gupta, R. Muthuraj and T. H. Mekonnen, *Green Chem.*, 2021, **23**, 5337–5378.
- 7 D. Wang, Z. Tang, R. Huang, Y. Duan, S. Wu, B. Guo and L. Zhang, *Chem. Mater.*, 2023, **35**, 764–772.
- 8 S. Fang, S. Yu, S. Wu, J. Wang, Z. Tang and B. Guo, *Compos. Sci. Technol.*, 2022, **225**, 109482.
- 9 M. Huang, J. Lu, B. Han, M. Qiu and L. Zhang, *Ind. Eng. Chem. Res.*, 2016, **55**, 9459–9467.
- 10 T. Liu, S. Jia, T. Kowalewski, K. Matyjaszewski, R. Casado-Portilla and J. Belmont, *Macromolecules*, 2006, **39**, 548–556.
- 11 A. Malas and C. K. Das, *Mater. Des.*, 2013, **49**, 857–865.
- 12 Y. Lei, B. Guo, X. Liu and D. Jia, *Appl. Surf. Sci.*, 2009, **255**, 8488–8493.
- 13 W. J. Chung, J. J. Griebel, E. T. Kim, H. Yoon, A. G. Simmonds, H. J. Ji, P. T. Dirlam, R. S. Glass, J. J. Wie, N. A. Nguyen, B. W. Guralnick, J. Park, Á. Somogyi, P. Theato, M. E. Mackay, Y.-E. Sung, K. Char and J. Pyun, *Nat. Chem.*, 2013, **5**, 518–524.
- 14 T. Lee, P. T. Dirlam, J. T. Njardarson, R. S. Glass and J. Pyun, *J. Am. Chem. Soc.*, 2022, **144**, 5–22.
- 15 B. Zheng, X. Wang, P. Lin, K. Chen, J. Chen, X. Lin, H. Shen and H. Zhang, *Langmuir*, 2025, **41**, 11614–11629.
- 16 B. Zheng, L. Zhong, X. Wang, P. Lin, Z. Yang, T. Bai, H. Shen and H. Zhang, *Nat. Commun.*, 2024, **15**, 5507.
- 17 H. Shen, B. Zheng and H. Zhang, *Polym. Rev.*, 2024, 1–56, DOI: [10.1080/15583724.2024.2382891](https://doi.org/10.1080/15583724.2024.2382891).
- 18 X. Chen, R. Zhang, Y. Mao, L. Zhong, P. Lin, Q. Deng, B. Zheng, H. Shen, Z. Feng and H. Zhang, *Chem. Eng. J.*, 2023, **467**, 143419.
- 19 J. J. Griebel, N. A. Nguyen, S. Namnabat, L. E. Anderson, R. S. Glass, R. A. Norwood, M. E. Mackay, K. Char and J. Pyun, *ACS Macro Lett.*, 2015, **4**, 862–866.
- 20 P. Yan, H. Wang, L. J. Dodd and T. Hasell, *Commun. Mater.*, 2023, **4**, 89.
- 21 A. P. Grimm, J. M. Scheiger, P. W. Roesky and P. Théato, *Polym. Chem.*, 2022, **13**, 5852–5860.
- 22 J. Wolfs, I. Ribca, M. A. R. Meier and M. Johansson, *ACS Sustainable Chem. Eng.*, 2023, **11**, 3952–3962.
- 23 Y. Jeon, J. Choi, D. Seo, S. H. Jung and J. Lim, *Polym. Chem.*, 2023, **14**, 1117–1123.
- 24 J. Wręczycki, D. M. Bieliński and R. Anyszka, *Polymers*, 2018, **10**, 870.
- 25 D. Wang, Z. Tang, Y. Liu and B. Guo, *Green Chem.*, 2020, **22**, 7337–7342.
- 26 S. Yu, Z. Tang, D. Wang, S. Wu, F. Chen, B. Guo and L. Zhang, *Polym. Chem.*, 2025, **16**, 1949–1960.
- 27 S. Zhang, Q. Yu, P. Liu, M. Guo, J. Ren, H. Li, Y. Hu and G. Zhou, *ACS Sustainable Chem. Eng.*, 2023, **11**, 18041–18050.
- 28 S. Zhang, P. Liu, M. Guo, Q. Yu, Y. Hu, Z. Tang, B. Guo and G. Zhou, *Compos. Sci. Technol.*, 2023, **239**, 110075.
- 29 K.-X. Hou, P.-C. Zhao, L. Duan, M. Fan, P. Zheng and C.-H. Li, *Adv. Funct. Mater.*, 2023, **33**, 2306886.
- 30 W. Sheard, K. W. Park and E. M. Leitao, *ACS Sustainable Chem. Eng.*, 2023, **11**, 3557–3567.
- 31 H. Shen, X. Chen, B. Zheng and H. Zhang, *ACS Appl. Polym. Mater.*, 2024, **6**, 14351–14364.
- 32 J. Cubero-Cardoso, A. A. Cuadri, F. G. Feroso, J. E. Martín-Alfonso and J. Urbano, *ACS Appl. Polym. Mater.*, 2022, **4**, 3667–3675.
- 33 D. Wang, Z. Tang, Z. Wang, L. Zhang and B. Guo, *Polym. Chem.*, 2022, **13**, 485–491.
- 34 Z. Wang, Y. Peng, L. Zhang, Y. Zhao, R. Vyzhimov, T. Tan and H. Fong, *Ind. Eng. Chem. Res.*, 2016, **55**, 2784–2789.
- 35 M. Jarnthong, N. Lopattananon, Y. Li, H. Yu, R. Wang, Y. Wang, H. Liu, L. Liao and Z. Peng, *ACS Sustainable Chem. Eng.*, 2024, **12**, 6440–6450.
- 36 J. Li, A. I. Isayev, X. Ren and M. D. Soucek, *Polymer*, 2015, **60**, 144–156.
- 37 X. Qin, Y. He, S. Khan, B. Zhang, F. Chen, D. Dong, Z. Wang and L. Zhang, *ACS Sustainable Chem. Eng.*, 2018, **6**, 12865–12871.
- 38 H. Xu, T. Fan, N. Ye, W. Wu, D. Huang, D. Wang, Z. Wang and L. Zhang, *Polymers*, 2020, **12**, 623.
- 39 C. Hayichelaeh and K. Boonkerd, *Ind. Crops Prod.*, 2024, **213**, 118451.
- 40 A. A. Hassan, K. Formela and S. Wang, *Compos. Sci. Technol.*, 2020, **197**, 108271.
- 41 A. D. Sarma, C. E. Federico, M. Staropoli, F. Nzulu, M. Weydert, P. Verge and D. F. Schmidt, *Ind. Crops Prod.*, 2021, **168**, 113600.
- 42 Z. Wang, Y. Han, Z. Huang, X. Zhang, L. Zhang, Y. Lu and T. Tan, *J. Appl. Polym. Sci.*, 2014, **131**, 40643.
- 43 Y. Hu, W. Dong and T. Masuda, *Macromol. Chem. Phys.*, 2013, **214**, 2172–2180.
- 44 S.-S. Choi and E. Kim, *Polym. Test.*, 2015, **42**, 62–68.
- 45 S. Zhang, X. Leng, Z. Li, L. Han, W. Li, C. Li, L. Lei, H. Ma and Y. Li, *Ind. Eng. Chem. Res.*, 2020, **59**, 10955–10966.
- 46 H. Berk, M. Kaya, M. Topcuoglu, N. Turkten, Y. Karatas and A. Cihaner, *React. Funct. Polym.*, 2023, **187**, 105581.
- 47 A. Hoefling, Y. J. Lee and P. Theato, *Macromol. Chem. Phys.*, 2017, **218**, 1600303.
- 48 A. A. Hassan, A. Abbas, T. Rasheed, M. Bilal, H. M. N. Iqbal and S. Wang, *Sci. Total Environ.*, 2019, **682**, 394–404.
- 49 C. Yan, A. Datta Sarma, E. Moretto, J.-S. Thomann, P. Verge, D. Schmidt, F. Kayser and R. Dieden, *Langmuir*, 2021, **37**, 10298–10307.
- 50 C. Peng, Q. Yang, W. Zhao, J. Ren, Q. Yu, Y. Hu and X. Zhang, *Compos. Sci. Technol.*, 2019, **177**, 103–110.
- 51 B. Zhong, Z. Jia, D. Hu, Y. Luo, D. Jia and F. Liu, *Composites, Part A*, 2017, **96**, 129–136.
- 52 J. Zhang, J. Qin, N. Wu, H. Feng, H. Wang, W. Zao, Y. Yang, Z. Liang and H. Zhang, *Polym. Compos.*, 2023, **44**, 980–991.
- 53 D. Wang, Z. Tang, S. Fang, S. Wu, H. Zeng, A. Wang and B. Guo, *Carbon*, 2021, **184**, 409–417.
- 54 A. P. Meera, S. Said, Y. Grohens and S. Thomas, *J. Phys. Chem. C*, 2009, **113**, 17997–18002.
- 55 X. He, M. Wu, S. Zhang, Q. Yu, P. Liu, Y. Zhang and Y. Hu, *Composites, Part A*, 2025, **191**, 108724.